EXPERIMENTAL OBSERVATION OF ISOLATED LARGE TRANSVERSE ENERGY ELECTRONS WITH ASSOCIATED MISSING ENERGY AT $\sqrt{s}$ = 540 GeV

The UA1 Collaboration

Presented by

D. LINGLIN

L.A.P.P., 74019 Annecy-le-Vieux (France)

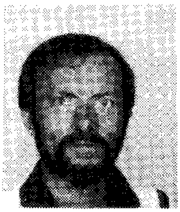

Abstract: We report the results of two searches made on data recorded at the CERN SPS Proton-Antiproton Collider: one for isolated large-E_T electrons, the other for large-E_T neutrinos using the technique of missing transverse energy. Both searches converge to the same events, which have the signature of a two-body decay of a particle of mass $\sim$ 80 GeV/c^2. The topology as well as the number of events fits well the hypothesis that they are produced by the process $\bar{p} + p \to W^\pm + X$, with $W^\pm \to e^\pm + \nu$; where $W^\pm$ is the Intermediate Vector Boson postulated by the unified theory of weak and electromagnetic interactions.

Résumé: Les résultats de deux recherches effectuées auprès du Collisionneur proton-antiproton du CERN sont présentés: la première concerne des électrons isolés ayant une grande énergie transverse, l'autre des neutrinos ayant également une grande $E_\perp$, en utilisant la technique de l'énergie transverse manquante. Les deux approches conduisent aux mêmes évènements, qui ont la signature de la désintégration 2-corps d'une particule de masse $\sim$ 80 GeV/c^2. La topologie aussi bien que le nombre d'évènements sont en accord avec l'hypothèse de la réaction $\bar{p}p \to W^\pm X$, avec $W^\pm \to e^\pm\nu$, où $W^\pm$ est le boson intermédiaire postulé par la théorie électro-faible.

1. INTRODUCTION

It is generally postulated that the beta decay, namely (quark) $\rightarrow$ (quark) + + $e^{\pm}$ + ν is mediated by one of two charged Intermediate Vector Bosons (IVBs), W^{+} and W^{-} of very large masses. If these particles exist, an enhancement of the cross-section for the process (quark) + (antiquark) $\rightarrow e^{\pm} + \nu$ should occur at centre-of-mass energies in the vicinity of the IVB mass (pole), where direct experimental observation and a study of the properties of such particles become possible. The CERN Super Proton Synchrotron (SPS) collider, in which proton and antiproton collisions at $\sqrt{s}$ = 540 GeV provide a rich sample of quark-antiquark events, has been designed with this search as the primary goal [1].

Properties of IVBs become better specified within the theoretical frame of the unified weak and electromagnetic theory and of the Weinberg-Salam model [2]. The mass of the IVB is precisely predicted [3]:

$$M_{W^{\pm}} = 82 \pm 2.4 \text{ GeV}/c^{2}$$

for the presently preferred [4] experimental value of the Weinberg angle $\sin^{2}\theta_{W}$ = = 0.23 ± 0.01. The cross-section for production is also reasonably well anticipated [5]

$$\sigma(p\bar{p} \rightarrow W^{\pm} \rightarrow e^{\pm} + \nu) \simeq 0.4 \times 10^{-33} \text{ k cm}^{2} \ ,$$

where k is an enhancement factor of ~ 1.5, which can be related to a similar well-known effect in the Drell-Yan production of lepton pairs. It arises from additional QCD diagrams in the production reaction with emission of gluons. In our search we have reduced the value of k by accepting only those events which show no evidence for associated jet structure in the detector.

2. THE DETECTOR

The UA1 apparatus has already been extensively described elsewhere [6]. Here we concentrate on those aspects of the detector which are relevant to the present investigation.

The detector is a transverse dipole magnet which produces a uniform field of 0.7 T over a volume of $7 \times 3.5 \times 3.5$ m^{3}. The interaction point is surrounded by the central detector (CD): a cylindrical drift chamber volume, 5.8 m long and 2.3 m in diameter, which yields a bubble-chamber quality picture of each $p\bar{p}$ interaction in addition to measuring momentum and specific ionization of all charged tracks.

Momentum precision for high-momentum particles is dominated by a localization error inherent to the system ($\leq 100\ \mu m$) and the diffusion of electrons drifting in the gas (proportional to $\sqrt{\ell}$ and about 350 μm after $\ell = 22$ cm maximum drift length). This results in a typical relative accuracy of ±20% for a 1 m long track at p = 40 GeV/c, and in the plane normal to the magnetic field. The precision, of course, improves considerably for longer tracks. The ionization of tracks can be measured by the classical method of the truncated mean of the 60% lowest readings to an accuracy of 10%. This allows an unambiguous identification of narrow, high-energy particle bundles (e^+e^- pairs or pencil jets) which cannot be resolved by the drift chamber digitizings.

The central section of electromagnetic and hadronic calorimetry has been used in the present investigation to identify electrons over a pseudorapidity interval $|\eta| < 3$ with full azimuthal coverage. Additional calorimetry, both electromagnetic and hadronic, extends to the forward regions of the experiment, down to 0.2° (for details, see table 1).

The central electromagnetic calorimeters consist of two different parts:

i) 48 semicylindrical modules of alternate layers of scintillator and lead (gondolas), arranged in two cylindrical half-shells, one on either side of the beam axis with an inner radius of 1.36 m. Each module extends over approximately 180° in azimuth and measures 22.5 cm in the beam direction. The light produced in each of the four separate segmentations in depth is seen by wavelength shifter plates on each side of the counter, in turn connected to four photomultipliers (PMs), two at the top and two at the bottom. Light attenuation is exploited in order to further improve the calorimetric information: the comparison of the pulse heights of the top and bottom PM of each segment gives a measurement of the azimuthal angle ϕ for localized energy depositions,

Table 1

Calorimetry

Calorimeter		Angular coverage θ (°)	Thickness		Cell size		Sampling step	Segmentation in depth	Resolution
			No. rad. lengths	No. abs. lengths	Δθ (°)	Δφ (°)			
Barrel	e.m.: gondolas	25-155	26/sin θ	1.1/sin θ	5	180	1.2 mm Pb 1.5 mm scint.	3.3/6.6/9.9/6.6 X_0	$0.15/\sqrt{E}$
	hadr.: c's		-	5.0/sin θ	15	18	50 mm Fe 10 mm scint.	2.5/2.5 λ	$0.8/\sqrt{E}$
End-caps	e.m.: bouchons	5-25	27/cos θ	1.1/cos θ	20	11	4 mm Pb 6 mm scint.	4/7/9/7 X_0	$0.12/\sqrt{E_T}$
	hadr.: I's	155-175	-	7.1/cos θ	5	10	50 mm Fe 10 mm scint.	3.5/3.5 λ	$0.8/\sqrt{E}$
Calcom	e.m.	0.7-5	30	1.2	4	45	3 mm Pb 3 mm scint.	4 × 7.5 X_0	$0.15/\sqrt{E}$
	hadr.	175-179.3	-	10.2	-	-	40 mm Fe 8 mm scint.	6 × 1.7 λ	$0.8/\sqrt{E}$
Very forward	e.m.	0.2-0.7	24.5	1.0	0.5	90	3 mm Pb 6 mm scint.	5.7/5.3/5.8/7.7 X_0	$0.15/\sqrt{E}$
	hadr.	179.3-179.8	-	5.7	0.5	90	40 mm Fe 10 mm scint.	5 × 1.25 λ	$0.8/\sqrt{E}$

$\Delta\phi$ (rad) = $0.3/\sqrt{E(GeV)}$. A similar localization along the beam direction is possible using the complementary pairing of PMs. The energy resolution for electrons using all four PMs is $\Delta E/E = 0.15/\sqrt{E(GeV)}$.

ii) 64 petals of end-cap electromagnetic shower counters (bouchons), segmented four times in depth, on both sides of the central detector at 3 m distance from the beam crossing point. The position of each shower is measured with a position detector located inside the calorimeter at a depth of 11 radiation lengths, i.e. after the first two segments. It consists of two planes of orthogonal proportional tubes of 2 × 2 cm^2 cross-section and it locates the centre of gravity of energetic electromagnetic showers to ±2 mm in space. The attenuation length of the scintillator has been chosen to match the variation of sin θ over the radius of the calorimeters, so as to directly measure in first approximation $E_T = E \sin\theta$ rather than the true energy deposition E, which can, however, be determined later, using the information from the position detector. This technique permits us to read out directly from the end-cap detectors the amount of transverse energy deposited, without reconstruction of the event topology.

3. ELECTRON IDENTIFICATION

Electromagnetic showers are identified by their characteristic transition curve, and in particular by the lack of penetration in the hadron calorimeter behind them. The performance of the detectors with respect to hadrons and electrons has been studied extensively in a test beam as a function of the energy, the angle of incidence, and the location of impact. The fraction of hadrons (pions) delivering an energy deposition E_c below a given threshold in the hadron calorimeter is a rapidly falling function of energy, amounting to about 0.3% for $p \simeq 40$ GeV/c and $E_c < 200$ MeV. Under these conditions, 98% of electrons are detected.

4. NEUTRINO IDENTIFICATION

The emission of one (or more) neutrinos can be signalled only by an apparent visible energy imbalance of the event (missing energy). In order to permit such a measurement, calorimeters have been made completely hermetic down to angles of 0.2° with respect to the direction of the beams. (In practice, 97% of the mass of the magnet is calorimetrized.) It is possible to define an energy flow vector $\vec{\Delta E}$, adding vectorially the observed energy depositions over the whole solid angle. Neglecting particle masses and with an ideal calorimeter response and solid-angle coverage, momentum conservation requires $\vec{\Delta E} = 0$. We have tested this technique on minimum bias and jet-enriched events for which neutrino emission ordinarily does not occur. The transverse components ΔE_y and ΔE_z exhibit small residuals centred on zero with an r.m.s. deviation well described by the law $\Delta E_{y,z} = 0.4\sqrt{\sum_i |E_T^i|}$, where all units are in GeV and the quantity under the square root is the scalar sum of all transverse energy contributions recorded in the event (fig. 1). The distributions have Gaussian shape and no prominent tails. The longitudinal component of energy ΔE_x is affected by the energy flow escaping through the 0° singularity of the collider's beam pipe and it cannot be of much practical use. We remark that, like neutrinos, high-energy muons easily penetrate the calorimeter and leak out substantial amounts of energy. A muon detector, consisting of stacks of eight planes of drift chambers, surrounds the whole apparatus and has been used to identify such processes, which are occurring at the level of 1 event per nanobarn for $\Delta E_{y,z} \geq 10$ GeV.

5. DATA-TAKING AND INITIAL EVENT SELECTIONS

The present work is based on data recorded in a 30-day period during November and December 1982. The integrated luminosity after subtraction of dead-time and other instrumental inefficiencies was 18 nb^{-1}, corresponding to about 10^9 collisions between protons and antiprotons at $\sqrt{s} = 540$ GeV.

For each beam-beam collision detected by scintillator hodoscopes, the energy depositions in all calorimeter cells after fast digitization were processed, in the time prior to the occurrence of the next beam-beam crossing, by a fast arithmetic processor in order to recognize the presence of a localized electromagnetic energy deposition, namely of at least 10 GeV of transverse energy either in two gondola elements or in two bouchon petals. In addition, we have simultaneously

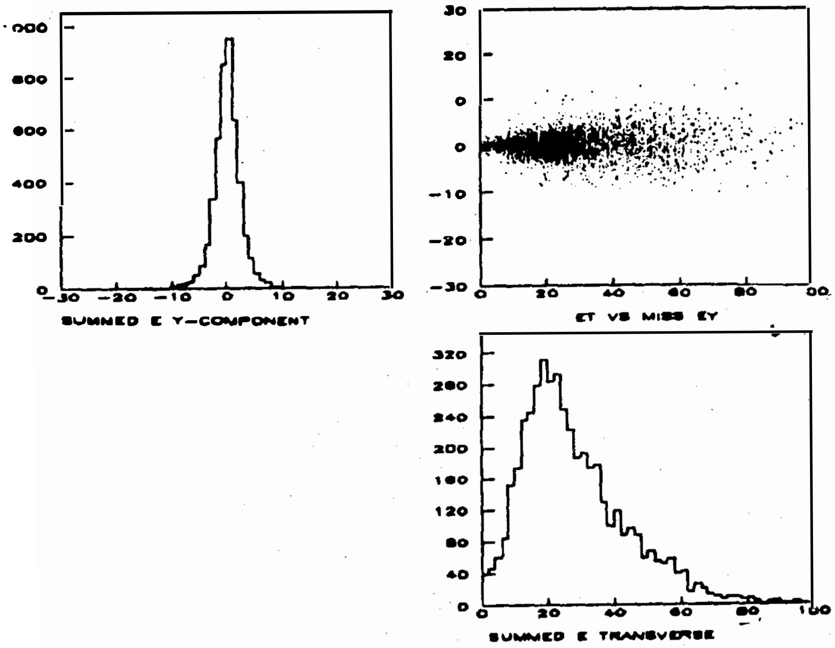

Fig. 1

The missing transverse energy in the y direction [ΔE_y (GeV)] plotted versus the scalar sum of missing transverse energy [E_T (GeV)] for minimum bias triggers. The y-axis is pointing up vertically.

operated three other trigger conditions: i) a jet trigger, with ≥ 15 GeV of transverse energy in a localized cluster [7] of electromagnetic and hadron calorimeters; ii) a global E_T trigger, with > 40 GeV of total transverse energy from all calorimeters with $|\eta| < 1.4$; and iii) a muon trigger, namely at least one penetrating track with $|\eta| < 1.3$ pointing to the diamond.

The electron trigger rate was about 0.2 event per second at the (peak) luminosity $L = 5 \times 10^{28}$ cm^{-2} s^{-1}. Collisions with residual gas or with vacuum chamber walls were completely negligible, and the apparatus in normal machine conditions yielded an almost pure sample of beam-beam collisions. In total, 9.75×10^5 triggers were collected, of which 1.4×10^5 were characterized by an electron trigger flag.

Event filtering by calorimetric information was further perfected by off-line selection of 28,000 events with $E_T > 15$ GeV in two gondolas, or $E_T > 15$ GeV in two bouchon petals with valid position-detector information. These events were finally processed with the central detector reconstruction. Of these events there are 2125 with a good quality, vertex-associated charged track of $p_T > 7$ GeV/c. This sample will be used for the subsequent analysis of events in the gondolas.

6. SEARCH FOR ELECTRON CANDIDATES

We now require three conditions in succession in order to ensure that the track is isolated, namely to reject the debris of jets:

i) The fast track ($p_T > 7$ GeV/c) as recorded by the central detector must hit an pair of adjacent gondolas with transverse energy $E_T > 15$ GeV (1106 events).

ii) Other charged tracks, entering the same pair of gondolas, must not add up to more than 2 GeV/c of transverse momenta (276 events).

iii) The ϕ information from pulse division from gondola phototubes must agree within 3σ with the impact of the track (167 events).

Next we introduce two simple conditions to enhance its electromagnetic nature:

iv) The energy deposition E_c in the hadronic calorimeters aimed at by the track must not exceed 600 MeV (72 events).

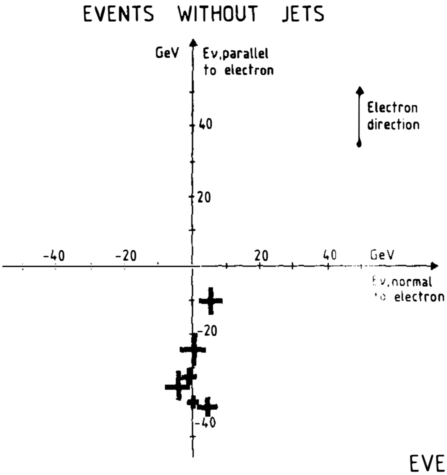

Fig. 2a

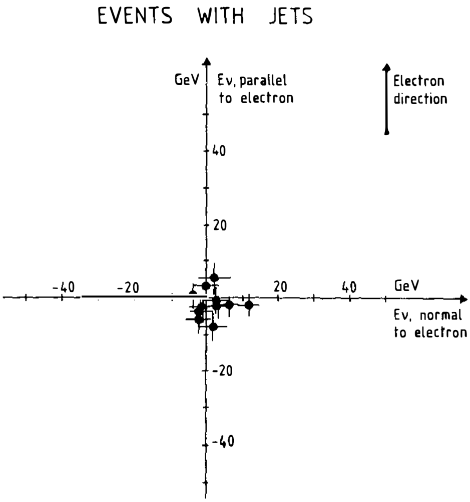

Fig. 2b

The missing transverse energy (E_ν) is plotted vectorially against the electron direction for the events yielded by the electron search: a) without jets, b) with jets.

v) The energy deposited in the gondolas E_{gon} must match the measurement of the momentum of the track p_{CD}, namely $|1/p_{CD} - 1/E_{gon}| < 3\sigma$.

At this point only 39 events are left, which were individually examined by physicists on the visual scanning and interactive facility Megatek. The surviving events break up cleanly into three classes, namely 5 events with no jet activity [8], 11 with a jet opposite to the track within a 30° angle in ϕ, and 23 with two jets (one of which contains the electron candidate) or clear e^+e^- conversion pairs. A similar analysis performed on the bouchon has led to another event with no jets. The classes of events have striking differences. We find that whilst events with jet activity have essentially no missing energy (fig. 2b) [9], the ones with no jets show evidence of a missing transverse energy of the same magnitude as the transverse electron energy (fig. 3a), with the vector momenta almost exactly balanced back-to-back (fig. 2a). In order to assess how significant the effect is, we proceed to an alternative analysis based exclusively on the presence of missing transverse energy.

7. SEARCH FOR EVENTS WITH ENERGETIC NEUTRINOS

We start again with the initial sample of 2125 events with a charged track of $p_T > 7$ GeV/c. We now move to pick up validated events with a high missing transverse energy and with the candidate track not part of a jet:

i) The track must point to a pair of gondolas with deposition in excess of $E_T > 15$ GeV and no other track with $p_T > 2$ GeV/c in a 20° cone (911 events).

ii) Missing transverse energy imbalance in excess of 15 GeV.

Only 70 events survive these simple cuts, as shown in fig. 4. The previously found 5 jetless events of the gondolas are clearly visible. At this point, as for the electron analysis, we process the events at the interactive facility Megatek:

iii) The missing transverse energy is validated, removing those events in which jets are pointing to where the detector response is limited, i.e. corners, light-pipe ducts going up and down. Some very evident, big secondary interactions in the beam pipe are also removed. We are left with 31 events, of which 21 have $E_c > 0.01\ E_{gon}$ and 10 events in which $E_c < 0.01\ E_{gon}$.

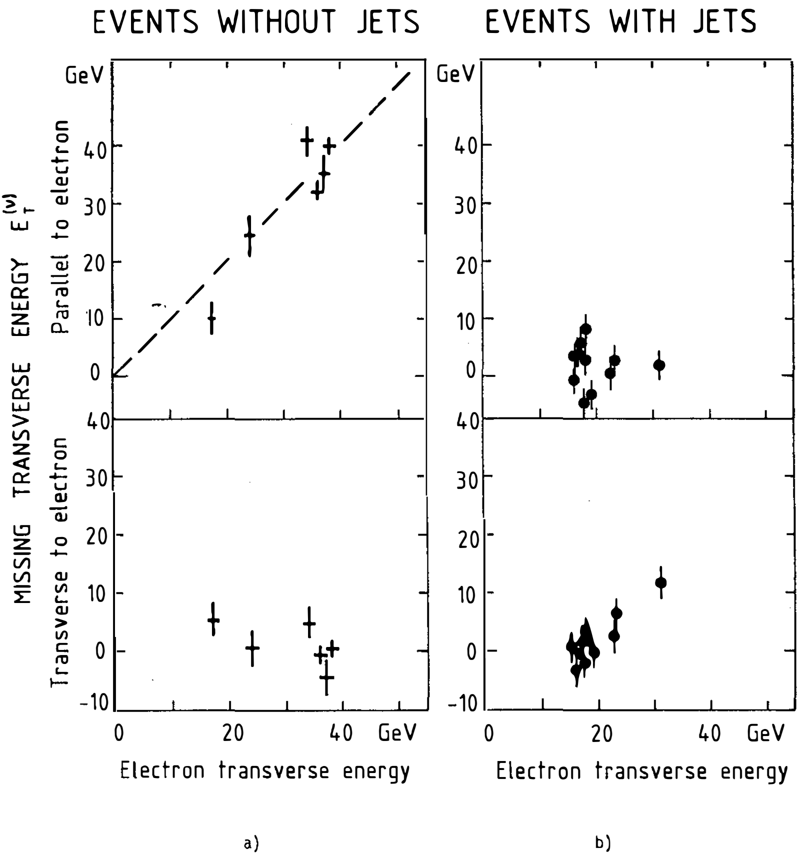

Fig. 3

The components of the missing energy parallel and perpendicular to the electron momentum plotted versus the electron energy for the events found in the electron search: a) without jets, b) with jets.

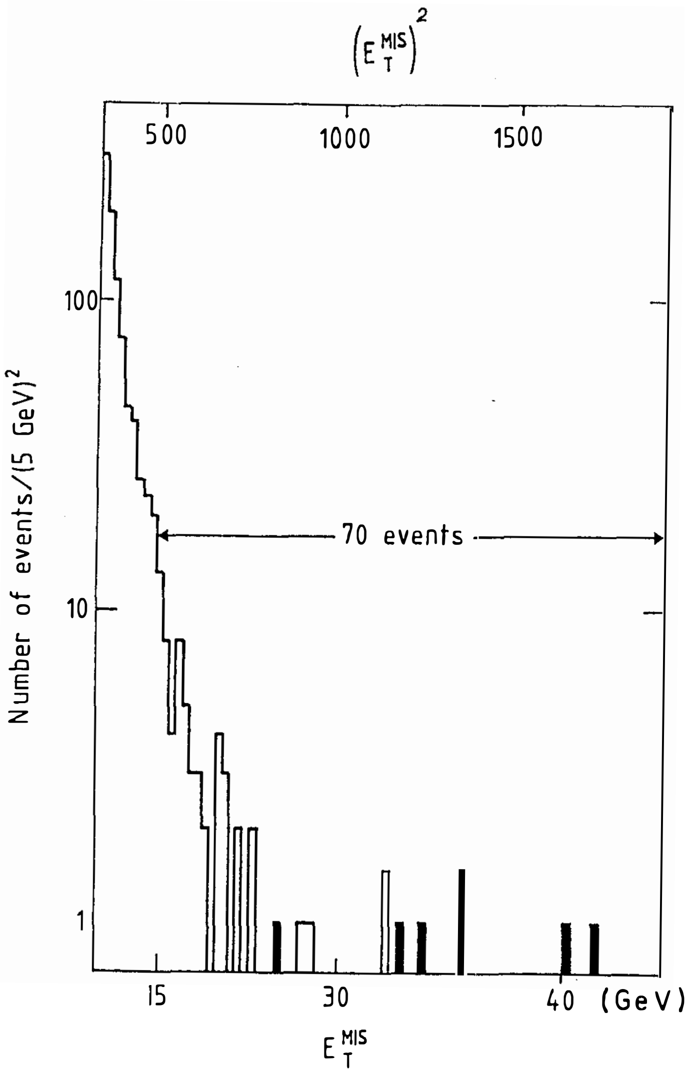

Fig. 4 : The distribution of the square of the missing transverse energy for those events which survive the cuts requiring association of the central detector isolated track and a struck gondola in the missing-energy search. The five jetless events from the electron search are indicated.

iv) We require that the candidate track be well isolated, that there is no track with $p_T > 1.5$ GeV in a cone of 30°, and that $E_T < 4$ GeV for neutrals in neighbouring gondolas at similar ϕ angle. Eighteen events survive: ten with $E_c \neq 0$ and eight with $E_c = 0$.

The events once again divide naturally into the two classes: 11 events with jet activity in the azimuth opposite to the track, and 7 events without detectable jet structure. If we now examine E_c, we see that these two classes are strikingly different, with large E_c for the events with jets (fig. 5b) and negligible E_c for the jetless ones (fig. 5a). We conclude that whilst the first ones are most likely to be hadrons, the latter constitute an electron sample.

We now compare the present result with the candidates of the previous analysis based on electron signature. We remark that five out of the seven events constitute the previous final sample (fig. 5a). Two new events have been added, eliminated previously by the test on energy matching between the central detector and the gondolas. Clearly the same physical process that provided us with the large-p_T electron delivers also high-energy neutrinos. The selectivity of our apparatus is sufficient to isolate such a process from either its electron or its neutrino features individually. If (ν_e, e) pairs and (ν_τ, τ) pairs are both produced at comparable rates, the two additional new events can readily be explained since missing energy can arise equally well from ν_e and ν_τ. Indeed, closer inspection of these events shows them to be compatible with the τ hypothesis, for instance, $\tau^- \to \pi^-\pi^0\nu_\tau$ with leading π^0. However, our isolation requirements on the charged track strongly biases against most of the τ decay modes.

8. DETAILED DESCRIPTION OF THE ELECTRON-NEUTRINO EVENTS

The main properties of the final sample of six events (five gondolas, one bouchon) are given in table 2 and marked A through F. The event G is a τ candidate. One can remark that both charges of the electrons are represented. The successive energy depositions in the gondola samples are consistent with test beam findings. All but event D have no energy deposition in the hadron calorimeter; event D has a 400 MeV visible, 1% energy leakage beyond 25 radiation lengths. Test

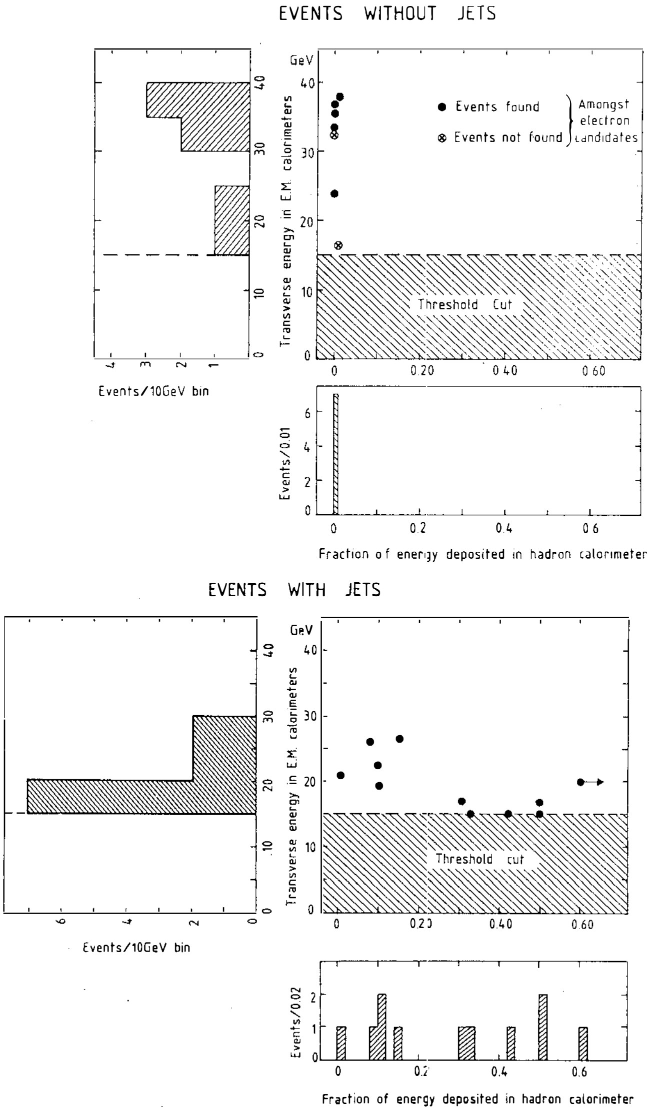

Fig. 5 : A plot of the transverse energy in the e.m. calorimeters versus the fraction of energy deposited in the hadron calorimeters for events which survive the missing-energy search: a) without jets, b) with jets.

<u>Table 2</u>

Main parameters of electron events with a large missing transverse energy

Run, event		Properties of the electron track										Calorimeter information					General event topology				
		E_T (GeV)	E (GeV)	p (GeV/c)	Δp a)	Q	dE/dx I/I_0	y b)	Track No.	Length (m)	Sagitta (mm)	Electromagnetic energy deposition: Sample 1 (GeV)	Sample 2 (GeV)	Sample 3 (GeV)	Sample 4 (GeV)	E_{had} (GeV)	E_{tot} (GeV)	Missing E_T (GeV)	Δφ c) (deg.)	Charged tracks	$\sum\lvert E_T\rvert$ (GeV)
A	2958 1279	24	39	33.8	$^{+6.3}_{-4.6}$	-	1.22 ±0.2	+1.1	36	1.36	1.7	3	34	2	0.2	0	278	24.4 ± 4.6	179	65	81
B	3522 214	17	46	47.5	$^{+8.2}_{-6.1}$	-	1.37 ±0.16	+1.7	18	1.64	1.5	2	32	10	0.5	0	296	11.6 ± 4.0	219	49	60
C	3524 197	34	45	21.6	$^{+21.8}_{-7.2}$	-	1.37 ±0.3	-0.8	26	1.25	2.11	1	30	14	0.2	0	367	41.3 ± 3.6	187	21	68
D	3610 760	38	40	33.4	$^{+33.0}_{-11.1}$	-	1.64 ±0.34	+0.3	9	0.98	0.75	3	9	26	2.2	0.4	111	40.0 ± 2.0	181	10	47
E	3701 305	37	37	56.2	$^{+121.3}_{-22.8}$	+	1.54 ±0.28	-0.1	12	0.95	0.4	1	18	17	0.9	0	363	35.5 ± 4.3	173	39	87
F	4017 838	36	70	53.1	$^{+6.6}_{-5.3}$	-	1.30 ±0.26	+1.4	3	2.01	2.0	19	48	3	0.3	0	177	32.3 ± 2.4	179	14	49
G	3262 1108	40	40	6.7	$^{+1.9}_{-1.2}$	-	1.23 ±0.28	0.0	21	0.85	3.0	2	22	15	0.9	0	218	33.4 ±2.9	172	21	63

a) Including 200 μm systematic error.

b) y is defined as positive in the direction of outgoing $\bar{p}$.

c) Angle between electron and missing energy (neutrino).

beam measurements show that this is a possible fluctuation. Multiplicity of the events is widely different: event F (fig. 6b, fig. 7b) has a small charged multiplicity (14), whilst event A (fig. 6a, fig. 7a) is very rich in particles (65). Event B is the bouchon event, and it has a number of features which must be mentioned. A 100 MeV/c track emerges from the vacuum chamber near the exit point of the electron track, which might form a part of an asymmetric electron pair with the candidate. The initial angle between the two tracks would then be 11°, not incompatible with this hypothesis once Coulomb scattering and measurement errors of the two tracks are taken into account. There is also some activity in the muon detector opposite to the electron candidate; the muon track is unmeasurable in the central detector. For these reasons we prefer to limit our final analysis to the events in the gondolas, although we believe that everything is still consistent with event B being a good event.

9. BACKGROUND EVALUATIONS

We first consider possible backgrounds to the electron signature for events with no jets. Missing energy (neutrino signature) is not yet advocated. We have taken the following into consideration:

1) A high-p_T charged pion (hadron) misidentified as an electron, or a high-p_T charged pion (hadron) overlapping with one or more π^0.

The central detector measurement obviously gives only the momentum p of the charged pion. In addition, the electromagnetic detectors can accumulate an arbitrary amount of electromagnetic energy from π^0's, which would simulate the electron behaviour. Since gondolas are thick enough to absorb the electromagnetic cascade, the energy deposition in the hadron calorimeter is dominated by the punch-through of the charged pion of momentum p measured in the central detector, for which rejection tables exist from test beam results. In our 18 nb^{-1} sample we have searched for single-track events with p_T > 20 GeV/c, no associated jet, E_c > > 600 MeV to ensure hadronic signature, and a reasonable energy balance (within 3 st. dev.) between the charged track momentum measurement and the sum of hadronic and electromagnetic energy depositions. We have found no such event. Once the

EVENT 2958. 1279.

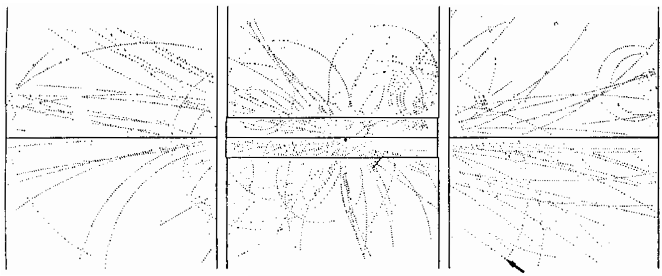

Fig. 6a

EVENT 4017. 838.

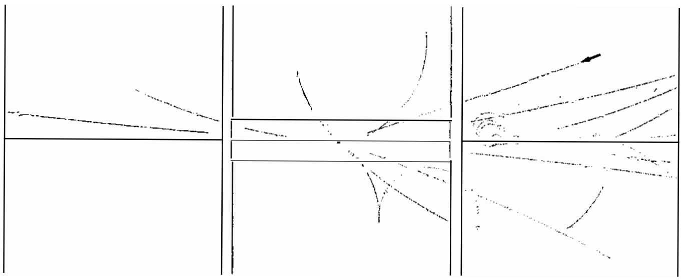

Fig. 6b

The digitizations from the central detector for the tracks in two of the events which have an identified, isolated, well-measured high-p_T electron: a) high-multiplicity, 65 associated tracks; b) low-multiplicity, 14 associated tracks.

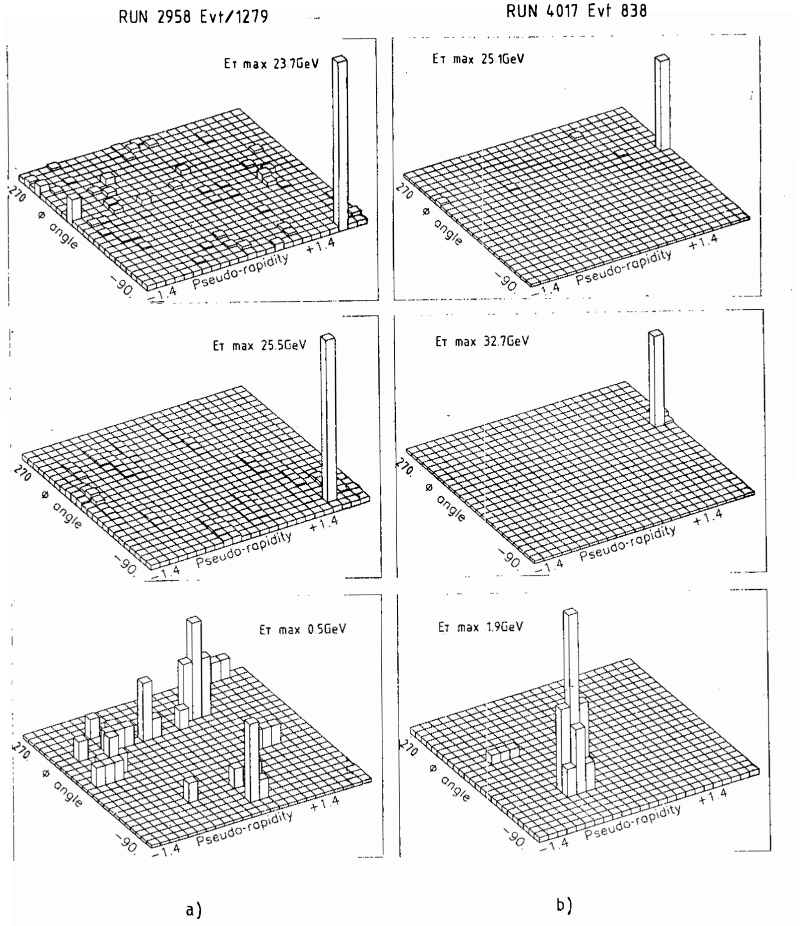

Fig. 7 : The energy deposited in the cells of the central calorimetry and the equivalent plot for track momenta in the central detector for the two events of fig. 6. The top diagram shows the electromagnetic cells, the middle shows the central detector tracks, and the bottom plot, with a very much increased sensitivity, shows the energy in the hadron calorimeter. The plots reveal no hadronic energy behind the electron and no jet structure; a) high multiplicity, b) low multiplicity.

measured pion rejection table is folded in, this background is entirely negligible. A further test against pile-up is given by the matching in the x-direction between the charged track of the central detector and the centroid of the energy depositions in the gondolas, and which is very good for all events.

2) High-p_T π^0, η^0, or γ internally (Dalitz) or externally converted to an e^+e^- pair with one leg missed. The number of isolated e.m. conversions (π^0, η, γ, etc.) per unit of rapidity has been directly measured as a function of E_T in the bouchons, using the position detectors over the interval 10-40 GeV. From this spectrum, the Bethe-Heitler formula for pair creation, and the Kroll-Wada formula for Dalitz pairs [10], the expected number of events with a "single" $e^{\pm}$ with $p_T >$ > 20 GeV/c is 0.2 p_0 (in GeV/c), largely independent of the composition of the e.m. component; p_0 is the effective momentum below which the low-energy leg of the pair becomes undetectable. Very conservatively, we can take p_0 = 200 MeV/c (curvature radius 1.2 m) and conclude that this background is negligible.

3) Heavy quark associated production, followed by pathological fragmentation and decay configuration, such that $Q_1 \to e(\nu X)$ with the electron leading and the rest undetected, and $Q_2 \to \nu(\ell X)$, with the neutrino leading and the rest undetected. In 5 nb^{-1} we have observed one event in which there is a muon and an electron in separate jets, with $p_T^{(\mu)}$ = 4.4 GeV/c and $p_T^{(e)}$ = 13.3 GeV/c. Requiring i) extrapolation to the energy of the events, ii) fragmentation functions for leading lepton, and iii) a detection hole for all remaining particles, makes the rate of these background events negligible.

In conclusion, we have been unable to find a background process capable of simulating the observed high-energy electrons. Thus we are led to the conclusion that they are electrons. Likewise we have searched for backgrounds capable of simulating large-E_T neutrino events. Again, none of the processes considered appear to be even near to becoming competitive.

10. COMPARISON BETWEEN EVENTS AND EXPECTATIONS FROM W DECAYS

The simultaneous presence of an electron and (one) neutrino of approximately equal and opposite momenta in the transverse direction (fig. 8) suggests the presence of a two-body decay, $W \to e + \nu_e$. The main kinematical quantities of the events are given in table 3. A lower, model-independent bound to the W mass m_W can be obtained from the transverse mass, $m_T^2 = 2p_T^{(e)} p_T^{(\nu)} (1 - \cos \phi_{\nu_e})$, remarking that $m_W \geq m_T$ (fig. 9). We conclude that:

$$m_W > 73 \text{ GeV/c}^2 \text{ (90\% confidence level)} .$$

A better accuracy can be obtained from the data if one assumes W decay kinematics and standard V-A couplings. The transverse momentum distribution of the W at production also plays a role. We can either i) extract it from the events (table 3); or, ii) use theoretical predictions [11].

As one can see from fig. 10, there is good agreement between two extreme assumptions of a theoretical model [11] and our observations. By requiring no associated jet, we may have actually biased our sample towards the narrower first-order curve. Fitting of the inclusive electron spectrum and using full QCD smearing gives $m_W = 74 {}^{+4}_{-4}$ GeV/c^2. The method finally used is the one of correcting, on an event-to-event basis, for the transverse W motion from the $(E_\nu - E_e)$ imbalance, and using the Drell-Yan predictions with no smearing. The result of a fit on electron angle and energy and neutrino transverse energy with allowance for systematic errors, is

$$m_W = 81 {}^{+5}_{-5} \text{ GeV/c}^2 ,$$

in excellent agreement with the expectation of the Weinberg-Salam model [2].

We find that the number of observed events, once detection efficiencies are taken into account, is in agreement with the cross-section estimates based on structure functions, scaling violations, and the Weinberg-Salam parameters for the W particle [5].

Table 3

Transverse mass and transverse momentum of a W decaying into an electron and a neutrino computed from the events of table 2

Run, event	$p_T^{(e)}$ of electron (GeV/c)	$p_T^{(\nu)}$ = missing E_T (GeV)	Transverse mass (GeV/c^2)	$p_T^{(W)} = \lvert \vec{p}_T^{(e)} + \vec{p}_T^{(\nu)} \rvert$ (GeV)
A 2958 1279	24 ± 0.6	24.4 ± 4.6	48.4 ± 4.6	0.6 ± 4.6
B 3522 214	17 ± 0.4	11.6 ± 4.0	26.5 ± 4.6	10.8 ± 4.0
C 3524 197	34 ± 0.8	41.3 ± 3.6	74.8 ± 3.4	8.6 ± 3.7
D 3610 760	38 ± 1.0	40.0 ± 2.0	78.0 ± 2.2	2.1 ± 2.2
E 3701 305	37 ± 1.0	35.5 ± 4.3	72.4 ± 4.5	4.7 ± 4.4
F 4017 838	36 ± 0.7	32.3 ± 2.4	68.2 ± 2.6	3.8 ± 2.5

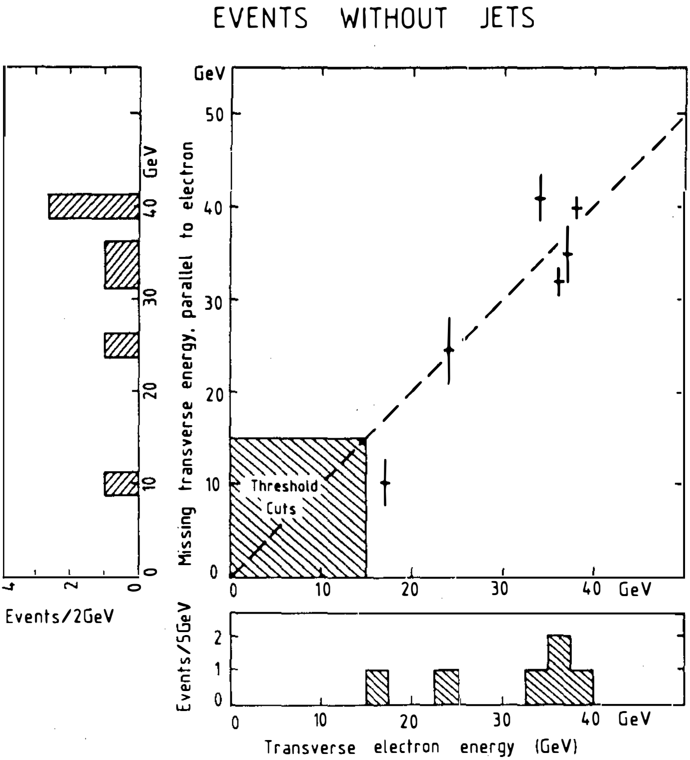

Fig. 8

The missing transverse energy component parallel to the electron, plotted versus the transverse electron energy for the final six electron events without jets (5 gondolas, 1 bouchon). All the events in the gondolas appear well above the threshold cuts used in the searches.

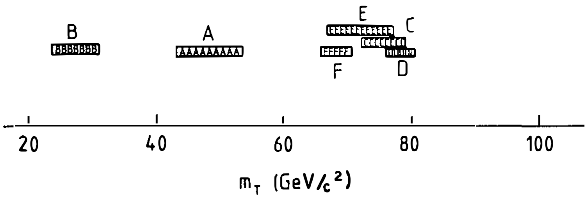

Fig. 9

The distribution of the transverse mass derived from the measured electron and neutrino vectors of the six electron events.

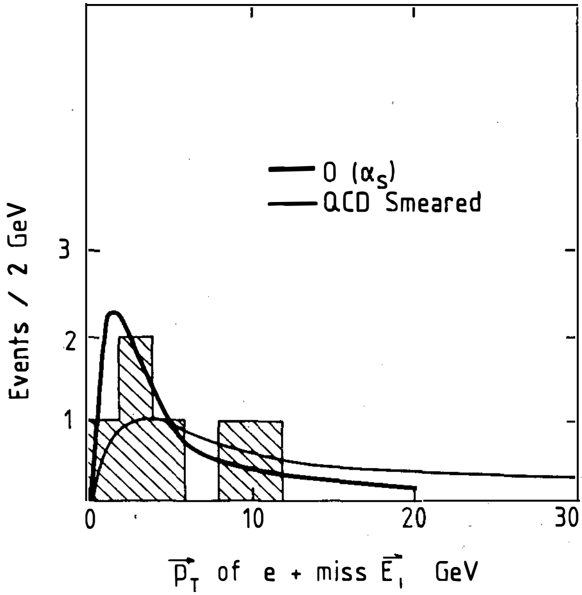

Fig. 10

The transverse momentum distribution of the W derived from our events, using the electron and missing-energy vectors. This is compared with the theoretical predictions of Halzen et al. [11] for W production without [$O(\alpha_s)$] and with QCD smearing.

Acknowledgements

We gratefully acknowledge J.B. Adams and L. Van Hove, CERN Directors-General during the initial phase of the project and without whose enthusiasm and support our work would have been impossible. The success of the collider run depended critically upon the superlative performance of the whole of the CERN accelerator complex, which was magnificantly operated by its staff.

We are thankful to the management and staff of CERN and of all participating Institutes who have vigorously supported the experiment.

The following funding Agencies have contributed to this programme:

Fonds zur Förderung der Wissenschaftlichen Forschung, Austria.

Valtion luonnontieteellinen toimikunta, Finland.

Institut National de Physique Nucléaire et de Physique des Particules and Institut de Recherche Fondamentale (CEA), France.

Bundesministerium für Forschung und Technologie, Germany.

Istituto Nazionale di Fisica Nucleare, Italy.

Science and Engineering Research Council, United Kingdom.

Department of Energy, USA.

Thanks are also due to the following people who have worked with the collaboration in the preparation and data collection on the runs described here, F. Bernasconi, F. Cataneo, A.-M. Cnops, L. Dumps, J.-P. Fournier, A. Micolon, S. Palanque, P. Quéru, P. Skimming, G. Stefanini, M. Steuer, J.C. Thevenin, H. Verweij and R. Wilson.

REFERENCES AND FOOTNOTES

[1] C. Rubbia, P. McIntyre and D. Cline, Proc. Int. Neutrino Conference, Aachen, 1976 (Vieweg, Braunschweig, 1977), p. 683.

Study Group, Design study of a proton-antiproton colliding beam facility, CERN/PS/AA 78-3 (1978), reprinted in Proc. Workshop on Producing High-Luminosity, High-Energy Proton-Antiproton Collisions, Berkeley, 1978 (report LBL-7574, UC34c), p. 189.

The staff of the CERN proton-antîproton project, Phys. Lett. 107B (1981) 306.

[2] S. Weinberg, Phys. Rev. Lett. 19 (1967) 1264.

A. Salam, Proc. 8th Nobel Symposium, Aspenäsgården, 1968 (Almqvist and Wiksell, Stockholm, 1968), p. 367.

[3] A. Sirlin, Phys. Rev. D 22 (1980) 971.

W.J. Marciano and A. Sirlin, Phys. Rev. D 22 (1980) 2695.

C.H. Llewellyn Smith and J.A. Wheater, Phys. Lett. 105B (1981) 486.

[4] For a review, see M. Davier, Proc. 21st Int. Conf. on High-Energy Physics, Paris, 1982 [J. Phys. (France), No. 12, t. 43, 1982], p. C3-471.

[5] F.E. Paige, Proc. Topical Conference on the Production of New Particles at Super-High Energies, Univ. Wisconsin, Madison, 1979.

L.B. Okun and M.B. Voloshin, Nucl. Phys. B120 (1977) 459.

C. Quigg, Rev. Mod. Phys. 94 (1977) 297.

J. Kogut and J. Shigemitsu, Nucl. Phys. B129 (1977) 461.

R. Horgan and M. Jacob, Proc. CERN School of Physics, Malente (FRG), 1980 (CERN 81-04), p. 65.

R.F. Peierls, T. Trueman and L.L. Wang, Phys. Rev. D 16 (1977) 1397.

[6] UA1 proposal: A 4π solid-angle detector for the SPS used as a proton-antiproton collider at a centre-of-mass energy of 540 GeV, CERN/SPSC 78-06 (1978).

M. Barranco Luque et al., Nucl. Instrum. Methods 176 (1980) 175.

M. Calvetti et al., Nucl. Instrum. Methods 176 (1980) 255.

K. Eggert et al., Nucl. Instrum. Methods 176 (1980) 217 and 233.

A. Astbury, Phys. Scr. 23 (1981) 397.

[7] We define a cluster as: i) a group of eight gondolas and the two hadron calorimeter elements immediately behind; or ii) a quadrant of bouchon elements (8) with the corresponding hadron calorimeters.

[8] The definition of a jet is based on the UA1 standard algorithm, applied separately on the calorimetry and on the central detector data. Positive results on either set are taken as evidence for a jet. In the calorimetry a four-vector $(\vec{k}_i, E_i)$ pointing to the interaction vertex is associated with each struck cell. Working in the transverse plane, all vectors with $k_T > 2.5$ GeV are ordered and are used as potential jet initiators. They are combined if their separation in phase space satisfies the cut $\Delta R = \sqrt{(\Delta\eta)^2 + (\Delta\phi)^2} < 1$ ($\Delta\phi$ in radians). The remaining soft particles are added to the nearest jet in $\Delta\eta$ and $\Delta\phi$, provided the relative p_T is < 1 GeV and $\Delta\theta < 45°$. A jet is considered valid if $E_T^{jet} > 10$ GeV. This same procedure is used for central detector tracks with appropriately adjusted parameters.

[9] The 11 events with an electron and a jet exhibit a p_T^{-4} spectrum with the highest event at $p_T = 32$ GeV/c.

[10] H.M. Kroll and W. Wada, Phys. Rev. 98 (1955) 1355.

[11] F. Halzen and D.M. Scott, Phys. Lett. 78B (1978) 318.
P. Aurenche and F. Lindfors, Nucl. Phys. B185 (1981) 301.
F. Halzen, A.D. Martin, D.M. Scott and M. Dechantsreiter, Phys. Lett. 106B (1981) 147.
M. Chaichian, M. Hayashi and K. Yamagishi, Phys. Rev. D 25 (1982) 130.
A. Martin, Proc. Conf. on Antiproton-Proton Collider Physics, Madison, 1981 (AIP Proceedings No. 85, 1982), p. 216.
F. Halzen, A.D. Martin and D.M. Scott, Phys. Rev. D 25 (1982) 754.
V. Barger and R.J.N. Phillips, University of Wisconsin preprint MAD/PH/78 (1982).